Gas Discharge Lamps Are Volatile Memristors

Deyan Lin, *Member, IEEE*, S. Y. Ron Hui, *Fellow, IEEE*, and Leon O. Chua, *Life Fellow, IEEE*

***Abstract*—Discharge lamps can be classified as high-pressure and low-pressure lamps, which operate under different scientific principles. They have exhibited the well-known fingerprints of memristors. This paper describes the mathematical models of both of high- and low-pressure discharge lamps based on their respective physical nature and behaviors, and then explains how these models can be unified into a generalized mathematical framework that confirms their memristor characteristics. Practical and theoretical results from high-pressure and low-pressure lamps are included to illustrate their 3 fingerprints of the memristor characteristics. The results indicate that gas discharge lamps are not ideal but volatile memristors.**

***Index Terms*—Gas discharge devices, memristors, modeling.**

I. Introduction

MEMRISTOR, a two-terminal circuit element named by Leon Chua in 1971 [1] as a missing electric element, was realized by Hewlett Packard in 2008 and has been identified as "the fourth element" [2], [3]. With both resistive and memory properties, one main fingerprint of a memristor when subjected to a bipolar periodic signal is a pinched-hysteresis loop. This special feature has been explicitly observed in a number of devices including electric discharge lamps [4]. Hysteresis refers to the dependence of a system on the history of its state. It is a phenomenon observed in some systems and devices that possess inertia and memory [5]. The dynamic hysteresis characteristics of discharge lamps were observed by Reich and Depp in 1938 [6] and analyzed by V. J. Francis in 1948 [7]. Gas discharge lamps exhibit hysteresis in their voltage-current characteristics, because the time required for the ionization and deionization of gas molecules depends not only on the instantaneous current, but also on the past current and the rate of change of current.

In this paper, the physical nature and differences of high-pressure and low-pressure lamps are first addressed with the examples of a high-intensity discharge (HID) lamp (high-pressure type) and fluorescent lamps (low-pressure type) [8]–[15]. Their respective mathematical models are explained and then unified into a common mathematical framework. Finally, this framework is put into the memristor format for evaluation and confirmation of the memristor characteristics. Since the physics of discharge lamps has been well established and reported in the literature, this paper primarily focuses on the memristive aspects of the discharge lamps.

Manuscript received August 24, 2013; revised November 22, 2013; accepted December 24, 2013. Date of publication February 12, 2014; date of current version June 24, 2014. This work was supported by the University of Hong Kong, Imperial College London, the University of California, Berkeley, and in part by AFOSR Grant FA 9550-13-1-0136. This paper was recommended by Associate Editor R. Sipahi.

D. Lin is with the Department of Electrical & Electronic Engineering, University of Hong Kong, Pokfulam, Hong Kong (e-mail: deyanlin@eee.hku.hk).

S. Y. R. Hui is with the Departments of Electrical & Electronic Engineering, University of Hong Kong and Imperial College London, London, U.K., SW7 2AZ (e-mail: ronhui@eee.hku.hk).

L. Chua is with the Department of Electrical & Computer Engineering, University of California, Berkeley, CA USA 94720 (e-mail: chua@eecs.berkeley.edu).

Digital Object Identifier 10.1109/TCSI.2014.2304659

II. Memristor & Its Three Fingerprints

Ideal memristors can be classified as either charge-controlled or flux-controlled ones [3]. For a charge-controlled memristor, the relationship between the flux (φ) and charge (q) is [16]:

$$\varphi = f_M(q) \tag{1}$$

where $f_M(q)$ is a piecewise-differentiable function. The terminal current $i(t)$ and voltage $v(t)$ obey Ohm's Law:

$$v(t) = R(q) \cdot i(t) \tag{2}$$

and

$$R(q) = \frac{df_M(q)}{dq} \tag{3}$$

Whilst (1)–(3) use the resistor concept to describe the memristor, in general, "q" and "φ" can be other variables of a physical system that exhibits memristor characteristics and need not be charge and flux respectively.

The memristor studied in this paper is a natural extension of the ideal memristor, and is defined by:

$$v = R(x) \cdot i \tag{4}$$

$$\frac{dx}{dt} = f(x, i) \tag{5}$$

where v and i denote voltage and current respectively; the scalar state variable x denotes the gas temperature T_g in the high-pressure lamps and electron temperature T_e in the low-pressure lamps. Here $R(x)$ denotes the memristance in Ohms, $f(x, i)$ denotes a complicated nonlinear function of the state variable x and the device current i, along with other device parameters (to be defined in Section III).

The three fingerprints of memristors have been previously identified [16]–[18]. This section summarizes their properties.

A. Identical Zero-Crossing Property

The voltage waveform $v(t)$ and current waveform $i(t)$ of a memristor characterized by $0 < R(x) < \infty$ have identical zero-crossing points with the time axis (Fig. 1) [18], [19].

B. Pinched Hysteresis Loop Property

The i versus v loci corresponding to any periodic memristor waveforms $(v(t), i(t))$ must pass through the origin, and must have a typical hysteresis loop as shown in Fig. 2 [19], [20].

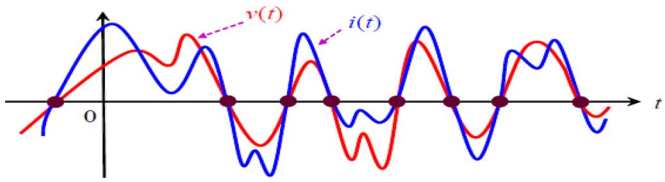

Fig. 1. Example of the $v(t)$ and $i(t)$ waveforms of a memristor with identical zero crossings. Image reproduced from [19].

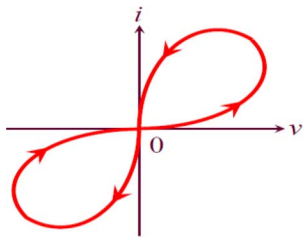

Fig. 2. Example of a pinched hysteresis loop [17], [18].

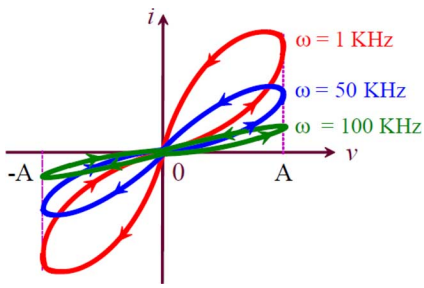

Fig. 3. Typical variations of the pinched hysteresis loop of a memristor as the frequency increases [19].

C. Frequency-Dependent Pinched Hysteresis Loop Property

The shape of the pinched hysteresis of a memristor varies with the frequency of the periodic input waveform and tends to a single line as the frequency $\rightarrow \infty$ [19], [20], as shown in Fig. 3. where A is the peak amplitude of input voltage v.

III. Physical Modeling of Gas Discharge Lamps

In order to evaluate the memristive nature of the discharge lamps, only physics-based mathematical models [8]–[15] will be used for this study. Curve-fitting and empirical lamp models are not considered. High-pressure and low-pressure lamps driven by practical circuits are used to confirm the validity of the models. There are two common types of driving circuits for gas discharge lamps, namely, the low-frequency magnetic ballast (Fig. 4(a)) and the high-frequency electronic ballast (Fig. 4(b)). The high-frequency ballast enables the operating frequency to be altered for dimming purpose. Such feature provides us a tool for evaluating the hysteresis loop of the V-I characteristics of both low-pressure and high-pressure discharge lamps.

A. High Pressure Discharge Lamp Model

In [10], the model for a high-intensity discharge (HID) lamp, which is a type of high-pressure lamps, is described with several physical equations. Unlike a low-pressure discharge lamp, the

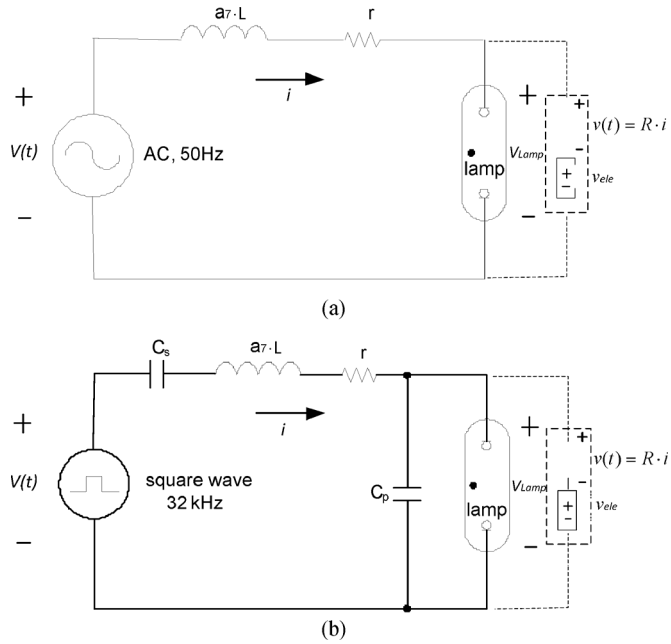

Fig. 4. Gas Discharge lamp operating circuit: (a) mains frequency magnetic ballast; (b) high-frequency electronic ballast (with the equivalent lamp circuit model represented in the dotted box).

discharge column of a HID lamp is under local thermal equilibrium. The energy balance equation applied to the discharge column of an HID lamp is:

$$\frac{dT_g}{dt} = a_1(i^2R - P_{\rm rad} - P_{\rm con}) \tag{6}$$

where T_g is the temperature of the gas inside the lamp tube when the HID lamp is under local thermal equilibrium (LTE) state [21], a_1 is a coefficient, i is the discharge current, R is the discharge arc resistance, $P_{\rm rad}$ is the radiation loss and$P_{\rm con}$ is the thermal conduction loss. The term i^2R can be considered as the input power to the lamp arc.

Under the local thermal equilibrium state, both Boltzmann [22] and Saha [23] equations can be applied to describe the excitation and ionization processes inside the lamp. The radiation loss equation based on the Boltzmann' formula with the assumption that the radiation is optically thin is:

$$P_{\rm rad} = a_2 \exp(-ea_3/kT_g) \tag{7}$$

where e is the magnitude of electron charge, k is the Boltzmann's constant; a_2 and a_3 are two coefficients. If the radiation is not optically thin, the contribution to the energy balance due to absorption of photons can be included in the thermal conductivity through the adjustment of the coefficient a_4 in the following thermal conduction loss equation:

$$P_{\rm con} = a_4(T_g - T_0) \tag{8}$$

where T_0 is the temperature at the wall of tube that contains the plasma discharge (typically around 1000 K). The lamp discharge resistance equation based on the Saha equation is:

$$R = \frac{l}{\int \sigma_e(T)dA} = a_5 T_g^{-\frac{3}{4}} \exp\left(\frac{ea_6}{2kT_g}\right) \tag{9}$$

TABLE I
ADJUSTABLE MODEL CONSTANTS FOR DIFFERENT TYPES OF LAMP

Lamp types	a_1	a_2	a_3	a_4	a_5	a_6	a_7
T8 36W	40225.4	119381.6	4.669	0.062	6529.46	0.264	1.232
HID 150W	20976.1	54350.4	0.986	0.128	2012.0	0.375	1.0

where l is the length of the arc discharge, A is the cross-sectional area of the arc, $\sigma_e(T)$ is the electrical conductivity of the arc discharge, and a_5 and a_6 are two coefficients.

When the lamp is driven by the ballast, the ballast circuit equation can be expressed as:

$$V(t) = a_7 L\frac{di}{dt} + i(R+r) + v_{\text{ele}} \tag{10}$$

where $V(t)$ is the input voltage of the ballast circuit, L is the ballast inductance, r is the ballast resistance and v_{ele} is the electrode voltage drop. Equations (6)–(9) do not include the effect of the loss rate of electrons by diffusion to the wall of the lamp tube. The coefficient a_7 is introduced to long tubular fluorescent lamps in [11]. For high-pressure lamps, however, the tube length is much shorter than fluorescent lamps. The ratio of the arc length and lamp tube diameter is normally low. The loss rate of electron by diffusion to the tube wall can therefore be ignored. The coefficient a_7 is 1.0 for HID lamps.

The model coefficients $a_1 - a_7$ for a 150 W HID lamp are listed in Table I. It is important to note that the ballast circuit is not part of the memristor. In the following figures, only the lamp characteristics such as voltage and current waveforms are displayed for evaluating their memristor characteristics. The lamp voltage is measured directly across the lamp terminals as shown in the equivalent lamp circuit in Fig. 4. It is equal to the sum of the lamp arc voltage and the electrode voltage drop. Mathematically, the lamp voltage (including the electrode voltage drop) is $v_{\text{lamp}}(t) = R\cdot i(t) + v_{\text{ele}}$. The lamp arc voltage is $v(t) = R\cdot i(t)$, where R is the lamp arc resistance.

For the high-frequency circuit in Fig. 4(b), the resonant capacitor *Cp* is used to create a high resonant voltage to ignite the lamp. Once the lamp is turned on, the lamp arc resistance is much smaller than the impedance of the resonant capacitor. Thus, the capacitor current is negligible. Fig. 5 shows the experimental and simulated lamp voltage and lamp current waveforms when the HID lamp is driven by a magnetic ballast at the mains frequency.

For the HID lamp, the profile of the electrode voltage drop for the positive half-cycle and the negative half-cycle can be mathematically approximated as:

$$v_{\text{ele}} = \begin{cases} Ae^{-Bt}\sin(2C\pi ft) + Dt & i > 0 \\ 0 & i = 0 \\ -Ae^{-Bt}\sin(2C\pi ft) - Dt & i < 0 \end{cases} \tag{11}$$

where the time variable t is reset to zero at the beginning of each half-cycle. A, B, C, and D are model parameters and f is the operating frequency [10]. According to [10], A is a constant value; B, C, and D are functions of frequency f : $A = 70, B = 8.3f + 1090, D = 4.8f + 761, C = 6$, when $f = 50$ Hz, else $C = 1$.

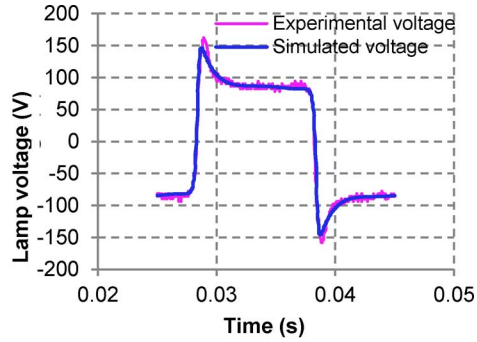

(a)

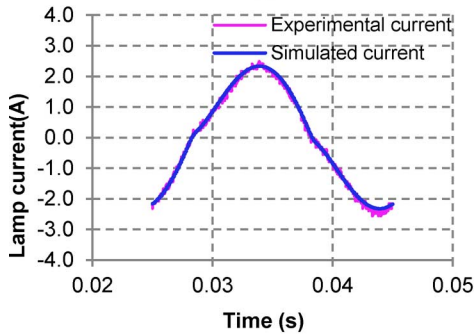

(b)

Fig. 5. Simulated and experimental lamp voltage and current waveforms of 150 W HID lamp at 50-Hz operating frequency: (a) lamp voltage; (b) lamp current.

B. Low Pressure Discharge Lamp Model

Unlike the HID lamp which is a high-pressure discharge lamp, a fluorescent lamp is a low-pressure discharge lamp which operates under a non-thermal equilibrium state. Therefore, the Saha equation does not apply to low-pressure lamps. The low-pressure discharge process cannot be described as a function of a single gas temperature as in the case of a high-pressure lamp (see (6)).

It has been pointed out [11] that the electron temperature T_e of a fluorescent lamp is much higher than the gas temperature T_g. The much higher electron temperature means that electrons are dominant in the energy conversion processes. Also, the elastic collision loss and UV radiation loss can occupy about 93% of the total energy losses. Thus, as an analogy to (6) for gas temperature, the energy balance equation for a fluorescent lamp in terms of the electron temperature can be expressed in the form of:

$$\frac{dT_e}{dt} = a_1(i^2R - P_{\text{rad}} - P_{\text{elastic}}) \tag{12}$$

where P_{elastic} is the elastic collision loss, P_{rad} is the UV radiative loss and a_1 is a coefficient.

The UV radiation power loss can be expressed as:

$$P_{\text{rad}} = a_2\exp(-ea_3/kT_e) \tag{13}$$

where a_2 and a_3 are coefficients and k is the Boltzmann's constant.

The elastic power loss is proportional to the electron temperature. It can be expressed as a linear function as follows:

$$P_{\text{elastic}} = a_4(T_e - T_g) \tag{14}$$

where a_4 is a coefficient and T_g is the gas temperature.

The electrical conductivity of a low-pressure discharge fluorescent lamp is proportional to the ionization rate per electron per atom. The dominant ionization process is a two-stage ionization which can be described as an algebraic and exponential function of the electron temperature [24]. When ignoring the algebraic dependence, the lamp arc resistance can be expressed as (15) [11]:

$$R = a_5 T_e^{-3/4} \exp(e a_6 / 2kT_e) \tag{15}$$

where a_5 and a_6 are lamp dependent coefficients.

Finally, the ballast circuit equation of the fluorescent lamp has the same format as that of the HID lamp,

$$V(t) = a_7 L \frac{di}{dt} + i(R + r) + v_{\text{ele}} \tag{16}$$

According to the plasma ionization balance equation, the rate of change of electron density is determined by the balance of the production rate of electrons by ionization and the loss rate of electrons by diffusion to the lamp tube. When compared with the high-pressure lamps, the low-pressure lamps such as the tubular fluorescent lamps are usually characterized by a very large ratio between arc length and lamp tube diameter. The smaller the lamp tube diameter is, the higher the loss rate of electrons caused by diffusion becomes. Equations (12)–(15) do not include the effect of the loss rate of electron by diffusion. When the lamp tube diameter is reduced, the predicted current will be higher than the experimental value. The coefficient a_7 is introduced in [11] to account for the loss rate of electrons by diffusion. It is equal to 1.0 for fluorescent lamps with large diameter (e.g., T12 lamps) in which the loss of electrons through diffusion is small. For fluorescent lamps with narrow tubes, a_7 is larger than 1.0 (e.g., $a_7 = 1.2$ for T8 lamps). Numerically, an a_7 higher than unity means that a smaller effective lamp voltage (i.e., $v_{\text{lamp}} = V(t) - a_7 L(di)/(dt) - ir$) appears across the lamp terminals. So a_7 accounts for the loss of electrons by diffusion in fluorescent lamps made of narrow tubes. The model coefficients a_1–a_7 for a T8 36 W fluorescent lamp are listed in Table I. Fig. 6 shows the experimental and simulated lamp voltage and lamp current waveforms for the circuit in Fig. 4(a). Again, their good agreement confirms the validity of the low-pressure discharge lamp model.

For the T8 36 W fluorescent lamp, the electrode voltage drop is:

$$v_{\text{ele}} = \begin{cases} 10\text{ V} & i > 0 \\ 0 & i = 0 \\ -10\text{ V} & i < 0 \end{cases} \tag{17}$$

The units for a_1 and a_4 are K/Ws and W/K respectively. Coefficients a_2, a_5, a_6 and a_7 have no unit.

C. Generalized Discharge Lamp Model Framework

Despite the fact that high-pressure and low-pressure discharge lamps operate under different lamp pressure and operating principles, it is important to note that their model equations have similar structures. Such similarities are also reflected by the similar waveforms in their lamp voltage and current. Table II compares the model equations of the HID (high-pressure) and fluorescent (low-pressure) lamps. The major difference is that the gas temperature T_g is used for the HID lamp model whilst the electron temperature T_e is used for the fluorescent lamp model.

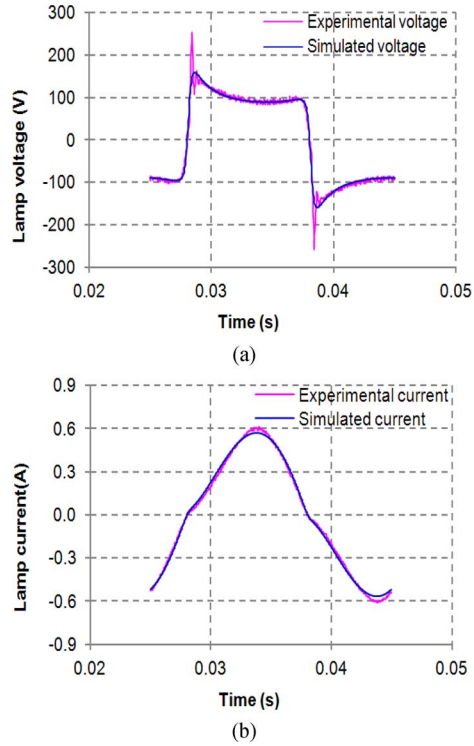

Fig. 6. Simulated and experimental lamp voltage and current waveforms of T8 36 W fluorescent lamp at 50-Hz operating frequency: (a) lamp voltage; (b) lamp current.

TABLE II
COMPARISON OF HID LAMP MODEL AND FLUORESCENT LAMP MODEL

HID lamp model (High-pressure discharge lamp model)	Fluorescent lamp model (Low-pressure discharge lamp model)
$\frac{dT_g}{dt} = a_1\left(i^2R - P_{rad} - P_{con}\right)$ (6)	$\frac{dT_e}{dt} = a_1\left(i^2R - P_{rad} - P_{elastic}\right)$ (12)
$P_{rad} = a_2 \exp\left(-ea_3 / kT_g\right)$ (7)	$P_{rad} = a_2 \exp\left(-ea_3/kT_e\right)$ (13)
$P_{con} = a_4\left(T_g - T_0\right)$ (8)	$P_{elastic} = a_4\left(T_e - T_g\right)$ (14)
$R = a_5 T_g^{-3/4} \exp\left(ea_6 / 2kT_g\right)$ (9)	$R = a_5 T_e^{-3/4} \exp\left(ea_6/2kT_e\right)$ (15)
$V(t) = a_7 L\frac{di}{dt} + i\left(R + r\right) + v_{ele}$ (10)	$V(t) = a_7 L\frac{di}{dt} + i\left(R + r\right) + v_{ele}$ (16)

Whilst the high-pressure and low-pressure discharge lamps are different in their scientific mechanisms in generating light, the same "mathematical" structures shown in Table II clearly indicate that a generalized set of model equations for both high-pressure and low-pressure discharge lamps can be formed. The equation set (6)–(10) has the same format as the equation set (12)–(16). This generalized discharge lamp model set will be turned into the memristor equation format in the next section for analysis.

Note that this generalized model can be applied not only to mains-frequency (50 H or 60 Hz) as shown in Fig. 5 for a HID lamp and Fig. 6 for a fluorescent lamp, but also to high-frequency operation as reported in [11].

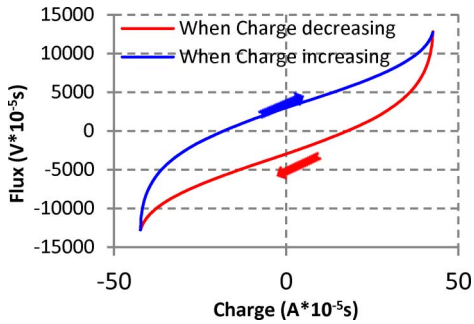

Fig. 7. Experimental φ-q curve of fluorescent lamp at mains frequency.

D. Generalized Discharge Lamp Model in Memristor Form

The generalized discharge lamp model equations are now used to check their three fingerprints of memristor as specified in [17]. Based on (4), the relationship between the discharge lamp arc voltage and current is:

$$v(t) = R(T) \cdot i(t) \tag{18}$$

where R is the lamp arc resistance which is:

$$R(T) = a_5 T^{-3/4} \exp(e a_6 / 2kT) \tag{19}$$

From (5) the scalar state variable x is T. Note that T is related to the current $i(t)$ through the following equation,

$$\begin{aligned} \frac{dT}{dt} &= f(T, i) \\ &= a_1[i(t)^2 R(t) - a_2 \exp(-e a_3/kT) - a_4 \exp(T - T_0)] \end{aligned} \tag{20}$$

For (18)–(20), T is the gas temperature T_g for high-pressure lamps and electron temperature T_e for low-pressure lamps; T_0 is the tube-wall temperature for high-pressure lamps and the gas temperature for low-pressure lamps. The charge $q(t)$ is related to the current by:

$$q(t) = \int_{-\infty}^{t} v(\tau)\, d\tau \tag{21}$$

The discharge process is a highly complex and nonlinear process. Equations (18)–(20) are coupled nonlinear equations and it is difficult to obtain a simple analytical solution. However, these equations can be solved numerically. Finally, the flux is expressed as:

$$\varphi = \int_{-\infty}^{t} v(\tau)\, d\tau \tag{22}$$

IV. Evaluation for Memristor Fingerprints

The generalized discharge lamp mathematical framework has been applied to a T8 36 W fluorescent lamp. Experimental and simulated characteristics of a T8 36 W fluorescent lamp are used to evaluate its memristor characteristics. These results are shown in Figs. 7 to 10. The lamp voltage includes the voltage across the lamp arc resistance and electrodes. All the experimental and simulated waveforms are captured when the root-mean-square value of the lamp current are controlled to 400 mA.

Since the flux versus charge curve in Fig. 7 is not a single-value curve, the discharge tube is not an ideal memristor, but a generalized memristor defined by a temperature-controlled memristance where the state variable $x = T_g$ for high-pressure lamps and $x = T_e$ for low-pressure discharge lamps.

For a memristor, the φ-q curve is one of the most important characteristics. Unlike some memristors with a single-valued φ-q curve, the T8 36 W fluorescent lamp has two different φ-q curves at mains frequency, one is for the increasing charge and the other one is for the decreasing charge, respectively, as shown in Fig. 7. Discharge lamps involve complicated processes of electro-chemical, ionization, species diffusion inside the lamp tube during the lamp operation [10], [15].

The 3 fingerprints of a memristor [16], [19] are:

i. Identical zero-crossing property;
ii. Pinched hysteresis loop property;
iii. Frequency-dependent pinched hysteresis loop property.

All of these properties can be evaluated with the use of the Lissajous figure [25]. By using the model mentioned in Section III, practical tests and simulations have been conducted to obtain the voltage-current Lissajous figures of the T8 36 W fluorescent lamp for a wide frequency range from 5 Hz to 32 kHz. Figs. 8(a)–(e), show the measured and simulated results for the Lissajous figures obtained at 5 Hz, 50 Hz, 300 Hz, 1 kHz and 32 kHz, respectively. Several important points can be observed.

1) All the voltage-current Lissajous figures of the discharge lamps are pinched at the origin. This is the identical zero-crossing property and the first fingerprint of a memristor.
2) Hysteresis loops are observed in the dynamic voltage-current Lissajous figures, except at very low-frequency close to dc operation (such as 5 Hz in Fig. 8(a)) and at very high-frequency (such as 32 kHz in Fig. 8(e)). So the second fingerprint of a memristor that device exhibits pinched hysteresis property is confirmed.
3) The lobe area of the hysteresis loop initially increases from very low frequency. After reaching a certain value, it reduces as operating frequency increases. The hysteresis loop approaches a single-valued curve as the frequency becomes very high (Fig. 8(e)). The frequency dependency of the lobe area is thus confirmed. However, the proposed model does not capture the nonlinearity of the i-v_{lamp} curve when the lamp is under high frequency operation.

To further examine the memristor characteristic of the discharge lamp and accuracy of the generalized mathematical framework, the measured Lissajous figures at different frequencies in Fig. 9(a) are compared with their simulated ones in Fig. 9(b). These results confirm the accuracy of the generalized discharge lamp model framework except some nonlinear effects at high frequencies.

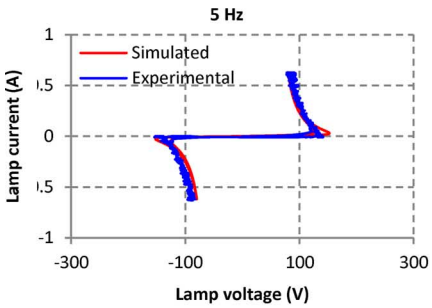

a

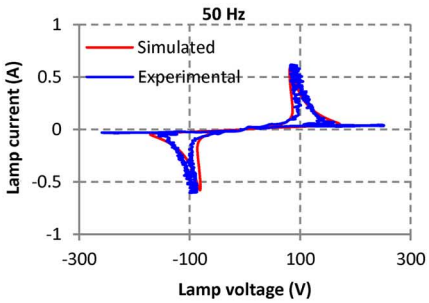

b

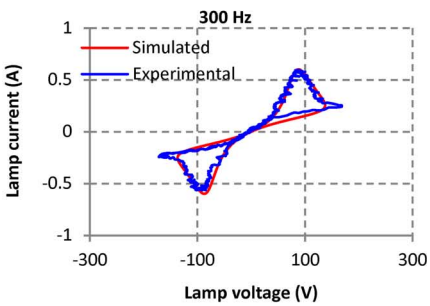

c

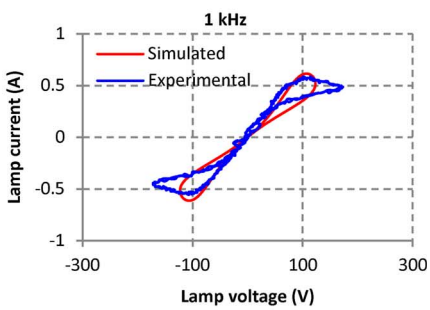

d

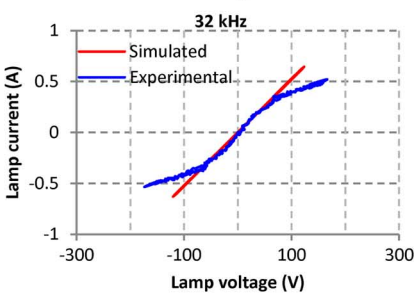

e

Fig. 8. (a) Experimental and Simulated V-I hysteresis loop of the fluorescent lamp operating at 5 Hz, (b) Experimental and Simulated V-I hysteresis loop of the fluorescent lamp operating at 50 Hz, (c) Experimental and Simulated V-I hysteresis loop of the fluorescent lamp operating at 300 Hz, (d) Experimental and Simulated V-I hysteresis loop of the fluorescent lamp operating at 1 kHz, (e) Experimental and Simulated V-I hysteresis loop of the fluorescent lamp operating at 32 kHz.

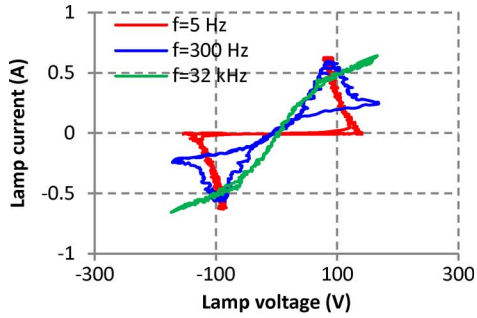

(a)

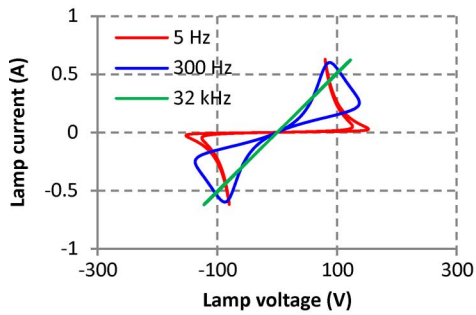

(b)

Fig. 9. V-I hysteresis loop comparison at 5 Hz, 300 Hz and 32 kHz for the T8 36 W fluorescent lamp: (a) experimental Lissajous figure; (b) simulated Lissajous figure.

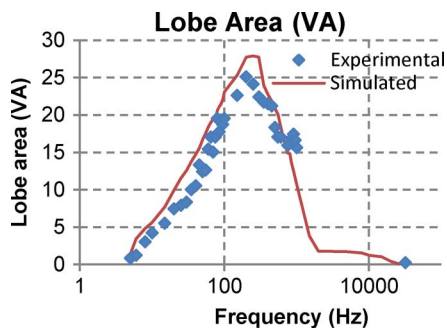

Fig. 10. Experimental and simulated V-I lobe area for a T8 36 W fluorescent lamp over a wide frequency range.

Now the hysteresis loop area of the T8 36 W fluorescent lamp is examined. The lobe area $A(f)$ can be obtained graphically from the V-I hysteresis loops recorded at different frequencies.

Fig. 10 shows the variation of the lobe area of the hysteresis of the T8 36 W fluorescent lamp from 5 Hz to 32 kHz when the rms value of the lamp current is kept at 400 mA. The lobe area increases from virtually zero at DC and reaches a maximum at about 300 Hz before it starts to decrease with increasing frequency. When the frequency reaches 32 kHz, the lobe area becomes very small. Further increase in frequency causes the lobe area to approach zero.

Under high frequency (32 kHz) operation, the V-I characteristics of the T8 fluorescent lamp over a dimming range (i.e., with different lamp current rms values) are recorded in Fig. 11(a). The corresponding simulated results are shown in Fig. 11(b). The averaged slopes of the measured curves can be determined from the two extreme points of the measurements. The averaged slopes of the measured and simulated curves are shown in

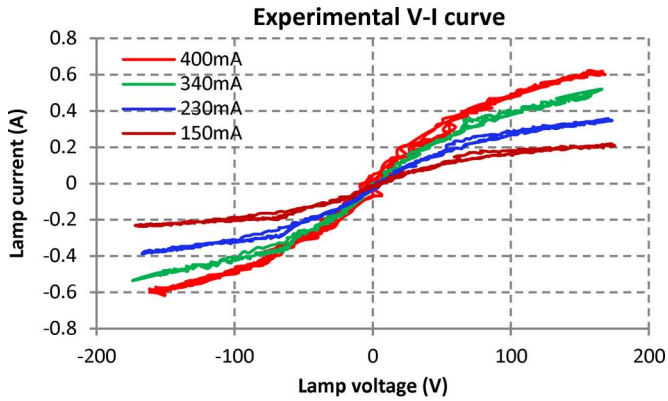

(a)

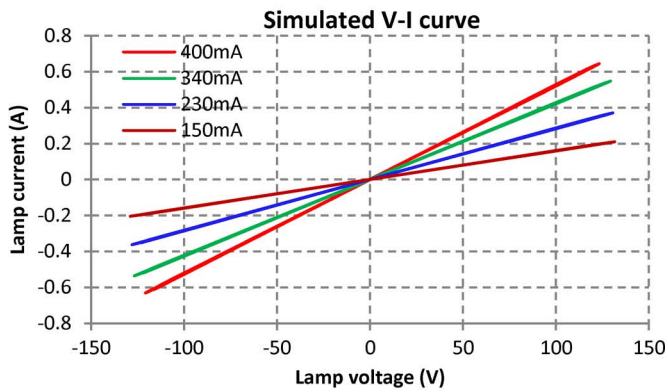

(b)

Fig. 11. Experimental and simulated V-I curves of the fluorescent lamp at 32 kHz over a dimming range: (a) experimental curves; (b) simulated curves.

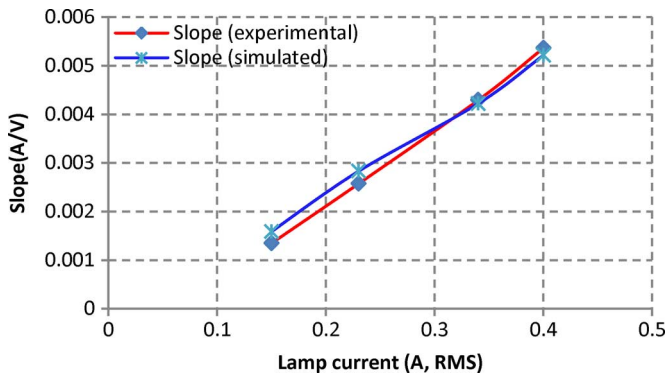

Fig. 12. Relationship of the slopes of the V-I curves at 32 kHz over a dimming range.

Fig. 12. The good agreements between the measured and theoretical results confirm the validity of the generalized mathematical framework of discharge lamps for memristor studies.

V. Conclusion

Discharge lamps exhibit memristor characteristics as pointed out previously [4]. Due to the highly complex and nonlinear nature, there has not been a generalized mathematical framework to prove that all discharge lamps (i.e., both high-pressure and low-pressure gas discharge lamps) are memristors. This paper fills this theoretical gap by generalizing a mathematical framework that suits both high-pressure and low-pressure lamps, despite their different physical operating principles. Such a framework is then studied in the mathematical format of a memristor. The generalized discharge lamp framework offers theoretical results that satisfy the three fingerprints of a memristor. Practical results obtained from a discharge lamp have been included to confirm the validity of the proposed mathematical framework.

Since the simulated results are based on the generalized discharge lamp model, the mathematical framework provided in this paper offers the theoretical basis to support the idea that all discharge lamps, regardless of being high-pressure or low-pressure, are memristors. As the ionized state of the gas inside a discharge lamp will revert to the neutral state when the excitation is removed, the operating point will return to the origin of the v_{lamp}-i plot. Therefore, discharge lamps are strictly speaking volatile memristors.

References

[1] L. Chua, "Memristor—The missing circuit element," *IEEE Trans. Circuit Theory*, vol. 18, pp. 507–519, 1971.
[2] O. Kavehei, K. Yeong-Seuk, A. Iqbal, K. Eshraghian, S. F. Al-Sarawi, and D. Abbott, "The fourth element: Insights into the memristor," in *Proc. ICCCAS*, 2009, pp. 921–927.
[3] L. O. Chua, "The fourth element," *Proc. IEEE*, vol. 100, pp. 1920–1927, 2012.
[4] T. Prodromakis, C. Toumazou, and L. Chua, "Two centuries of memristors," *Nature Materials*, vol. 11, pp. 478–481, 2012, 06//print.
[5] Y. V. Pershin and M. Di Ventra, "Memory effects in complex materials and nanoscale systems," *Adv. Phys.*, vol. 60, pp. 145–227, Apr. 01, 2011, 2011.
[6] H. J. Reich and W. A. Depp, "Dynamic characteristics of glow discharge tubes," *J. Appl. Phys.*, vol. 9, pp. 421–426, June 1938, 00.
[7] V. J. Francis, *Fundamentals of Discharge Tube Circuits*. London: Methuen, 1948.
[8] W. Yan, S. Y. R. Hui, and H. Chung, "Nonlinear high-intensity discharge lamp model including a dynamic electrode voltage drop," in *IEE Proc.—Science, Measurement and Technol.*, 2003, vol. 150, pp. 161–167.
[9] W. Yan and S. Y. R. Hui, "An improved high-intensity discharge lamp model including acoustic resonant effect on the lamp arc resistance," *IEEE Trans. Power Electron.*, vol. 19, pp. 1661–1667, 2004.
[10] Y. Wei and S. S. Y. R. Hui, "A universal PSpice model for HID lamps," *IEEE Trans. Industry Appl.*, vol. 41, pp. 1594–1602, 2005.
[11] W. Yan, E. Tam, and S. Y. Hui, "A semi-theoretical fluorescent lamp model for time-domain transient and steady-state simulations," *IEEE Trans. Power Electron.*, vol. 22, pp. 2106–2115, Nov. 2007.
[12] D. Y. Lin and W. Yan, "Modeling of cold cathode fluorescent lamps (CCFLs) with realistic electrode profile," *IEEE Trans. Power Electron.*, vol. 25, pp. 699–709, Mar. 2010.
[13] D. Lin, W. Yan, and S. Y. R. Hui, "Modelling the warm-up phase of the starting processes of high-intensity discharge lamps," *IET Science, Measurement Technol.*, vol. 5, pp. 199–205, 2011.
[14] D. Y. Lin, W. Yan, and S. Y. R. Hui, "Modeling of dimmable fluorescent lamp including the tube temperature effects," *IEEE Trans. Industrial Electron.*, vol. 58, pp. 4145–4152, Sept. 2011.
[15] D. Lin, W. Yan, G. Zissis, and S. Y. R. Hui, "Methodology for developing a low-pressure discharge lamp model with electron density variation and ambipolar diffusion," *IET Science, Measurement Technol.*, vol. 6, pp. 229–237, 2012.
[16] L. Chua, "Resistance switching memories are memristors," *Appl. Phys. A*, vol. 102, pp. 765–783, Mar. 01, 2011, 2011.
[17] S. P. Adhikari, M. P. Sah, H. Kim, and L. O. Chua, "Three fingerprints of memristor," *IEEE Trans. Circuits Syst.—I: Reg. Papers*, vol. PP, pp. 1–14, 2013.
[18] L. O. Chua and K. Sung Mo, "Memristive devices and systems," *Proc. IEEE*, vol. 64, pp. 209–223, 1976.
[19] L. Chua, V. Sbitnev, and H. Kim, "Hodgkin-Huxley Axon is made of memristors," *Int. J. Bifurcation Chaos*, vol. 22, p. 1230011, 2012.
[20] F. Corinto and A. Ascoli, "Memristive diode bridge with LCR filter," *Electron. Lett.*, vol. 48, pp. 824–825, 2012.
[21] J. F. Waymouth, "LTE and near-LTE lighting plasmas," *IEEE Trans. Plasma Sci.* , vol. 19, pp. 1003–1012, 1991.

[22] G. Zissis and K. Charrada, "Two-temperatures modelling of the high pressure Hg discharge lamp: Application to determination of the thermodynamic equilibrium state of the plasma," in *Proc. IEEE Int. Conf. Plasma Sci.* , 1996, p. 134.
[23] A. Anders, "Plasma fluctuations, local partial Saha equilibrium, and the broadening of vacuum-arc ion charge state distributions," *IEEE Trans. Plasma Sci.*, vol. 27, pp. 1060–1067, 1999.
[24] W. L. Lama, C. F. Gallo, T. J. Hammond, and P. J. Walsh, "Analytical model for low-pressure gas discharges: Application to the $\mathrm{Hg} + \mathrm{Ar}$ discharge," *Appl. Opt.*, vol. 21, pp. 1801–1811, May 15, 1982, 1982.
[25] M. P. Sah, H. Kim, and L. Chua, "Brains are made of memristors," *IEEE Circuits Syst. Mag.*, 2014, to be published.

Deyan Lin (M'09) was born in China in 1972. He received the B.Sc. and M.A.Sc. degrees from Huazhong University of Science and Technology, Wuhan, China, in 1995 and 2004, respectively, and the Ph.D. degree from the City University of Hong Kong, Kowloon, Hong Kong, in 2012.

He is currently a Research Associate with the Department of Electrical and Electronic Engineering, The University of Hong Kong, Pokfulam, Hong Kong.

From 1995 to 1999, he was a Teaching Assistant in Electrical Engineering Department at Jianghan University, Wuhan, where he became a Lecturer later. From 2008 to 2009, he was a Senior Research Assistant with the City University of Hong Kong. His current research interests include memristors, modeling and control of gas-discharge lamps, light-emitting diode technology and wireless power transfer.

S. Y. (Ron) Hui (M'87–SM'94–F'03) received the B.Sc. (Eng.) Hons. at the University of Birmingham, U.K., in 1984 and the D.I.C. and Ph.D. degrees from the Imperial College London, London, U.K., in 1987.

He has published over 270 technical papers, including more than 170 refereed journal publications and book chapters. Over 55 of his patents have been adopted by industry. He is an Associate Editor of the IEEE TRANSACTIONS ON POWER ELECTRONICS and the IEEE TRANSACTIONS ON INDUSTRIAL ELECTRONICS. Since 2013, he has been an Editor of the IEEE JOURNAL ON EMERGING AND SELECTED TOPICS IN POWER ELECTRONICS. His inventions on wireless charging platform technology underpin key dimensions of Qi, was the world's first wireless power standard, with freedom of positioning and localized charging features for wireless charging of consumer electronics.

Dr Hui received the IEEE Rudolf Chope R&D Award in 2010 from the IEEE Industrial Electronics Society and the IET Crompton Medal from the Institution of Engineering & Technology, UK. In the same year, he was elected to the Fellowship of the Australian Academy of Technological Sciences & Engineering. He currently holds Chair Professorships of Power Electronics at both of the University of Hong Kong and Imperial College London. He was appointed twice as an IEEE Distinguished Lecturer by the IEEE Power Electronics Society in 2004 and 2006.

Leon O. Chua (LF'in02) received the M.S. degree from the Massachusetts Institute of Technology, Cambridge, MA, USA, in 1961 and the Ph.D. degree from the University of Illinois at Champaign-Urbana, Urbana, IL, USA, in electrical engineering, in 1964.

He has been a Professor at the University of California Berkeley, Berkeley, CA, USA, since 1971. He was awarded seven patents and 14 honorary doctorates. When not immersed in science, he relaxes by searching for Wagner's leitmotifs, musing over Kandinsky's chaos, and contemplating Wittgenstein's inner thoughts.

Prof. Chua received many awards including the first recipient of the Gustav Kirchhoff Award, and the Guggenheim Fellow award. He was elected a foreign member of the Academia Europaea and of the Hungarian Academy of the Sciences. He was elected Confrerie des Chevaliers du Tastevin in 2000. In 2011, he was appointed a Distinguished Professor at the Technical University of Münich.